Mon. Not. R. Astron. Soc. **000**, 1–16 (2010) Printed 26 April 2013 (MN LATEX style file v2.2)

NGC 2579 and the carbon and oxygen abundance gradients beyond the solar circle⋆

C. Esteban[1,2]†, L. Carigi[3], M. V. F. Copetti[4,5], J. García-Rojas[1,2], A. Mesa-Delgado[6], H. O. Castañeda[7], D. Péquignot[5]

[1] *Instituto de Astrofísica de Canarias, E-38200 La Laguna, Tenerife, Spain*
[2] *Departamento de Astrofísica, Universidad de La Laguna, E-38206, La Laguna, Tenerife, Spain*
[3] *Instituto de Astronomía, Universidad Nacional Autónoma de México, Apdo. Postal 70-264, 04510 México D.F., Mexico*
[4] *Laboratório de Análise Numérica e Astrofísica, Departamento de Matemática, Universidade Federal de Santa Maria, 97119-900 Santa Maria, RS, Brazil*
[5] *LUTH, Observatoire de Paris-Meudon, 92190 Meudon, France*
[6] *Departamento de Astronomía y Astrofísica, Facultad de Física, Pontificia Universidad Católica de Chile, Av. Vicuña Mackenna 4860, 782-0436 Macul, Santiago, Chile*
[7] *Departamento de Física, Escuela Superior de Física y Matemática, Instituto Politécnico Nacional, México D.F., Mexico*

Accepted 2013 April 25. Received 2013 April 24; in original form 2013 March 13

ABSTRACT

We present deep echelle spectrophotometry of the Galactic H II region NGC 2579. The data have been taken with the Very Large Telescope Ultraviolet-Visual Echelle Spectrograph in the 3550–10400 Å range. This object, which has been largely neglected, shows however a rather high surface brightness, a high ionization degree and is located at a galactocentric distance of 12.4 ± 0.7 kpc. Therefore, NGC 2579 is an excellent probe for studying the behaviour of the gas phase radial abundance gradients in the outer disc of the Milky Way. We derive the physical conditions of the nebula using several emission line-intensity ratios as well as the abundances of several ionic species from the intensity of collisionally excited lines. We also determine the ionic abundances of C^{2+}, O^{+} and O^{2+} – and therefore the total O abundance – from faint pure recombination lines. The results for NGC 2579 permit to extend our previous determinations of the C, O and C/O gas phase radial gradients of the inner Galactic disc (Esteban et al. 2005) to larger galactocentric distances. We find that the chemical composition of NGC 2579 is consistent with flatten gradients at its galactocentric distance. In addition, we have built a tailored chemical evolution model that reproduces the observed radial abundance gradients of O, C and N and other observational constraints. We find that a levelling out of the star formation efficiency about and beyond the isophotal radius can explain the flattening of chemical gradients observed in the outer Galactic disc.

Key words: Galaxy: abundances – Galaxy: evolution – ISM: abundances – H II regions – ISM: individual: NGC 2579

1 INTRODUCTION

High-resolution spectroscopy with large aperture telescopes has permitted to measure very faint pure recombination lines (hereafter RLs) of heavy-element ions in Galactic and extragalactic H II regions (see García-Rojas & Esteban 2007; Peimbert 2003; López-Sánchez et al. 2007; Esteban et al. 2009). The brightest of these RLs are C II 4267 Å and those of multiplet 1 of O II about 4650 Å that can be used to determine the ionised gas phase C^{2+} and O^{2+} abundances, respectively. In H II regions, a systematic result is that abundances obtained with RLs are *always* between 1.5 to 3 times larger (the so-called abundance discrepancy factor, ADF) than those determined using the much brighter collisionally excited lines (hereafter CELs) of the same ions, C III] 1909 Å in the UV and those of [O III] in the optical (e.g. García-Rojas & Esteban 2007; Esteban et al. 2009). The origin of the abundance discrepancy (hereafter AD) is still an unsolved problem. Torres-Peimbert et al. (1980)

⋆ Based on observations collected at the European Southern Observatory, Chile, proposal number ESO 382.C-0195(A).
† E-mail: cel@iac.es

suggested that the presence of fluctuations in the spatial distribution of electron temperature can produce such discrepancy but others as Tsamis & Péquignot (2005) and Stasińska et al. (2007) consider that the AD may be produced by small spatial scale chemical inhomogeneities in the interstellar medium. Tsamis et al. (2011) have proposed that the presence of small and dense partially-ionised clumps along the line of sight are affecting the CEL-derived abundances, producing unrealistic lower values with respect to the RL-based ones, and a similar conclusion is found in the results by Mesa-Delgado et al. (2012). More recently, a new hypothesis based on the presence of a κ-distribution in the energy of the free electrons has been proposed to explain the AD (Nicholls et al. 2012).

From deep echelle spectra of a sample of Galactic H II regions, Esteban et al. (2005) determined the carbon and oxygen gradients of the Galactic disc at galactocentric distances between 6.3 and 10.4 kpc based on the intensity of RLs. Carigi et al. (2005) built chemical evolution models in order to reproduce those abundance gradients as well as other observational constraints. They found the important result that only models including carbon yields that increase with metallicity for massive stars and decrease with metallicity for low and intermediate mass stars can successfully reproduce simultaneously the gradients of both elements. Other result of that paper is that the fraction of carbon produced by massive stars with respect to that produced by low and intermediate mass stars strongly depends on the age of the Galactic disc, as well as on the galactocentric distance. Therefore, it is clear that similar C and O abundance data of H II regions at larger galactocentric distances are necessary to refine and extend chemical evolution models and explore possible changes across the Galactic disc.

There are some evidences that gas phase abundance gradients may flatten out at the outer parts of the Galactic disc (Fich & Silkey 1991; Vílchez & Esteban 1996; Maciel & Quireza 1999; Costa et al. 2004; Maciel et al. 2006). However, this result is not supported by other studies (Deharveng et al. 2000; Rudolph et al. 2006; Henry et al. 2010; Balser et al. 2011). Chemical evolution models of the Galactic disc also obtain different solutions for the behaviour of the abundance gradients at large galactocentric distances. For example, Fu et al. (2009) find a steepening of the gradients as radial distances increase and Marcon-Uchida et al. (2010) can predict a flattening or a steeping depending on the assumed behaviour of the star formation efficiency across the Galactic disc. Moreover, chemodynamical models of Samland et al. (1997) also predict the development of a plateau in the outer regions of the Galaxy. Therefore, the finding of indisputable observational evidence of the presence or not of such flattening is essential to increase our knowledge on important ingredients of chemical evolution models such as the timescale for disc formation and the density threshold for star formation.

NGC 2579 is a high surface brightness Galactic H II region that has been largely neglected because its misclassification as either planetary nebula (Acker et al. 1992) or reflection nebula (van den Bergh & Herbst 1975) and even its confusion with other nearby objects (Archinal & Hynes 2003). Copetti et al. (2007) have brought into attention the interest of NGC 2579 presenting the first comprehensive observational study of the nebular properties and stellar content of this object. These authors derive consistent photometric and kinematic distances for NGC 2579 indicating that it is located at a galactocentric distance of 12.4 ± 0.7 kpc (assuming the Sun at 8 kpc from the Galactic Centre). Therefore, NGC 2579 is probably the brightest H II region located at that distant part of the Galaxy, well outside the solar circle. Another remarkable characteristic of this nebula is its relatively high ionization degree, which facilitates the determination of chemical abundances and the determination of C^{2+} and O^{2+} abundances from RLs. Undoubtedly, NGC 2579 is an excellent probe for the exploration of the behaviour of the ionised gas phase radial abundance gradients in the external parts of the Galactic disc.

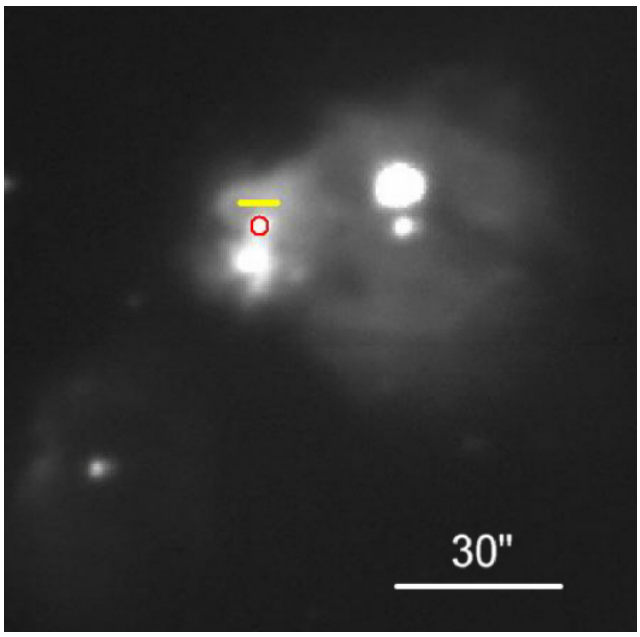

Figure 1. Combination of Hα and continuum image of NGC 2579. The position of the reference star DENIS J082054.8-361258 is indicated with a small circle. The grey (yellow) horizontal line centered at 5 arcsec to the north of the reference star indicates the area from which we extracted our one-dimensional spectra. North is up and east to the left.

In §2 we describe the observations and the data reduction procedure. In §3 we describe the emission line measurements and identifications as well as the reddening correction. In §4 we present the physical conditions and ionic and total abundances determined for NGC 2579. In §5 we describe the ingredients of our chemical evolution model and discuss the results in the light of the radial Galactic abundance gradients. Finally, in §6 we summarize our main conclusions.

2 OBSERVATIONS AND DATA REDUCTION

NGC 2579 was observed in service time on 2009 January 23 at Cerro Paranal Observatory (Chile), using the UT2 (Kueyen) of the Very Large Telescope (VLT) with the Ultraviolet Visual Echelle Spectrograph (UVES, D'Odorico et al. 2000). The standard settings of UVES were used covering the spectral range from 3570 to 10400 Å. Some small spectral intervals could not be observed. These are: 5734-5833 and 8425-8768 due to the physical separation between the

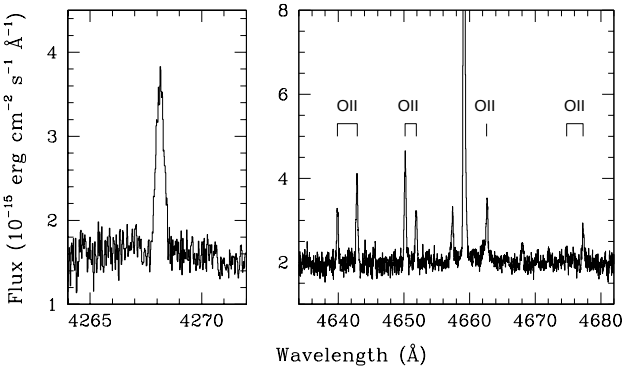

Figure 2. Sections of the UVES spectrum on NGC 2579 – uncorrected for reddening – showing the faint recombination lines of C II 4267 Å (left) and multiplet 1 of O II about 4650 Å (right).

CCDs of the detector system of the red arm; and several much smaller wavelength ranges between 8800 to 10400 Å because the last orders of the spectrum do not fit completely within the size of the CCD.

Three consecutive exposures of 400 seconds – for the 3570-3840 and 4820-6740 Å ranges – and of 1800 seconds – for the 3770-4940 and 6735-10400 Å ranges – each were added to obtain the final spectra. In addition, exposures of 30 and 60 seconds were taken to obtain non-saturated flux measurements for the brightest emission lines. The full width at half-maximum (FWHM) at a given λ was $\Delta\lambda \approx \lambda/8000$. The slit was oriented east-west and the atmospheric dispersion corrector (ADC) was used to keep the same observed region within the slit regardless of the air mass value. The slit width was set to $3''$ as a compromise between the spectral resolution needed and the desired signal-to-noise ratio of the spectra. The slit length was fixed to $10''$. The one-dimensional spectra we finally analysed were extracted for an area of $3''\times7''.4$. This area covers the brightest part of the nebula (see Figure 1), located $5''$ to the north of the star DENIS J082054.8-361258, a member of the stellar cluster that ionises the nebula.

The spectra were reduced using the IRAF[1] echelle reduction package, following the standard procedure of bias subtraction, aperture extraction, flatfielding, wavelength calibration and flux calibration. The standard star LTT 3218 (Hamuy et al. 1992, 1994) was observed to perform the flux calibration.

3 LINE INTENSITIES

Line fluxes were measured by integrating all the flux in the line between two given limits and over a local continuum estimated by eye. In the case of line blending, a double Gaussian profile fit procedure was applied to measure the individual line intensities. All these measurements were made with the SPLOT routine of IRAF.

All line fluxes of a given spectrum have been normalized to a particular bright emission line in each spectral range. For the bluest range (3570-3840 Å), the reference line was H12 3750 Å. For the 4820-6740 and 3770-4940 Å ranges, Hβ was used. For the reddest spectral interval (6735-10400 Å), the reference was P20 8392 Å. In order to produce a final homogeneous set of line flux ratios, all of them were rescaled to Hβ considering the theoretical H12/Hβ and P20/Hβ line ratios corresponding to the physical conditions of the gas.

The spectral ranges present some overlapping at the edges. The final flux of a line in the overlapping regions was the average of the values obtained in both adjacent spectra. A similar procedure was considered in the case of lines present in two consecutive spectral orders. The average of both measurements were considered as the adopted value of the line flux. In all cases, the differences in the line flux measured for the same line in different orders and/or spectral ranges do not show systematic trends and are always within the uncertainties.

The identification and laboratory wavelengths of the lines were obtained following our previous works on echelle spectroscopy of bright Galactic H II regions (see García-Rojas & Esteban 2007, and references therein). We also used a preliminar (unpublished) version of the spectral synthesis code for nebulae X-SSN (Péquignot et al. 2012) to identify faint lines. This code was specially useful to identify lines in the reddest part of the spectrum, where confusion with telluric features is problematic.

For a given line, the observed wavelength is determined by the centre of the baseline chosen for the flux integration procedures or the centroid of the line when a Gaussian fit is used (in the case of line blending). The final adopted values of the observed wavelength of a given line are relative to the heliocentric reference frame.

The reddening coefficient, $c(\mathrm{H}\beta)$, was determined from the comparison of the observed flux ratio of the brightest Balmer lines – Hα, Hγ, Hδ and Hν lines with respect to Hβ – and the theoretical line ratios computed by Storey & Hummer (1995) for the physical conditions of the nebula. We have used the reddening function, $f(\lambda)$, normalized to Hβ derived by Cardelli et al. (1989) and assuming $R_V = 3.1$. The c(Hβ) we obtain is 2.37±0.05, which is larger than the values of the reddening coefficient determined by Copetti et al. (2007) who use the reddening function by Kaler (1976) and obtain a range of values from 1.12 to 1.65 depending on the position inside the nebula and the Balmer lines used.

In Table 1, the final list of line identifications (columns 1–3), observed wavelength corrected for heliocentric velocity (column 4), observed and dereddened flux line ratios with respect to Hβ (columns 5 and 6) and the uncertainty of line ratios – in percentage – (last column) are presented. The quoted errors include the uncertainties in line flux measurement and error propagation in the reddening coefficient.

In Figure 2, we show sections of our flux-calibrated echelle spectra showing the recombination lines of C II 4267 Å and multiplet 1 of O II around 4650 Å. As it can be seen, these faint lines are well separated and show a remarkably high signal-to-noise ratio in our deep echelle spectrum.

[1] IRAF is distributed by NOAO, which is operated by AURA, under cooperative agreement with NSF.

Table 1. Observed, $F(\lambda)$, and reddening-corrected, $I(\lambda)$, line ratios [$F(\mathrm{H}\beta) = 100$] for NGC 2579.

λ_0 (Å)	Ion	Multiplet	λ_{obs} (Å)	$F(\lambda)$	$I(\lambda)$	Error (%)[a]
3587.28	He I	3	3588.08	0.039	0.180	17
3613.64	He I	6	3614.47	0.067	0.301	12
3634.25	He I	28	3635.07	0.052	0.227	14
3662.26	H I	H30	3663.19	0.045	0.192	16
3663.40	H I	H29	3664.21	0.036	0.154	18
3664.68	H I	H28	3665.54	0.056	0.238	14
3666.10	H I	H27	3666.90	0.059	0.254	13
3667.68	H I	H26	3668.54	0.076	0.327	12
3669.47	H I	H25	3670.31	0.080	0.343	11
3671.48	H I	H24	3672.31	0.088	0.377	11
3673.76	H I	H23	3674.60	0.090	0.384	11
3676.37	H I	H22	3677.20	0.114	0.483	10
3679.36	H I	H21	3680.21	0.156	0.663	8
3682.81	H I	H20	3683.62	0.138	0.581	9
3686.83	H I	H19	3687.68	0.126	0.531	9
3691.56	H I	H18	3692.42	0.186	0.779	8
3697.15	H I	H17	3697.98	0.250	1.042	7
3703.86	H I	H16	3704.71	0.262	1.085	7
3705.04	He I	25	3705.87	0.121	0.501	9
3711.97	H I	H15	3712.81	0.325	1.338	6
3721.83	[S III]	2F	3722.68	0.646	2.631	6
3721.94	H I	H14				
3726.03	[O II]	1F	3726.90	16.00	64.94	5
3728.82	[O II]	1F	3729.65	12.51	50.63	5
3734.37	H I	H13	3735.22	0.467	1.880	6
3750.15	H I	H12	3751.00	0.690	2.737	6
3770.63	H I	H11	3771.49	0.815	3.168	5
3797.90	H I	H10	3798.76	1.179	4.462	5
3819.61	He I	22	3820.49	0.262	0.969	7
3833.57	He I	62	3834.47	0.017	0.062	28
3835.39	H I	H9	3836.26	1.710	6.229	5
3856.02	Si II	1F	3856.90	0.026	0.093	22
3856.13	O II	12				
3862.59	Si II	1	3863.49	0.022	0.079	24
3867.49	He I	20	3868.34	0.042	0.150	16
3868.75	[Ne III]	1F	3869.64	3.409	11.99	5
3871.82	He I	60	3872.68	0.018	0.062	27
3888.65	He I	2	3889.85	3.911	13.46	5
3889.05	H I	H8				
3918.98	C II	4	3919.82	0.008	0.028	:
3920.68	C II	4	3921.50	0.023	0.076	23
3926.53	He I	58	3927.42	0.035	0.114	18
3964.73	He I	5	3965.63	0.289	0.914	6
3967.46	[Ne III]	1F	3968.37	1.131	3.567	5
3970.07	H I	H7	3970.97	4.912	15.45	5
4009.22	He I	55	4010.19	0.067	0.203	12
4026.21	He I	18	4027.12	0.733	2.161	5
4068.60	[S II]	1F	4069.56	0.239	0.670	7
4069.62	O II	10	4070.66	0.033	0.092	19
4072.15	O II	10	4073.05	0.022	0.063	24
4075.86	O II	10	4076.81	0.021	0.058	25
4076.35	[S II]	1F	4077.32	0.075	0.209	12
4101.74	H I	H6	4102.67	9.500	25.60	5
4120.82	He I	16	4121.72	0.085	0.225	11
4143.76	He I	53	4144.72	0.136	0.347	8
4153.3	O II	19	4154.29	0.012	0.030	36
4168.97	He I	52	4169.96	0.019	0.048	26
4267.15	C II	6	4268.14	0.071	0.157	12
4287.40	[Fe II]	7F	4288.40	0.013	0.027	34
4317.14	O II	2	4318.07	0.010	0.021	39
4326.4	O I		4327.45	0.010	0.021	38

Table 1. continued

λ_0 (Å)	Ion	Multiplet	λ_{obs} (Å)	$F(\lambda)$	$I(\lambda)$	Error (%)[a]
4340.47	H I	Hγ	4341.45	23.67	47.27	4
4345.56	O II	2	4346.57	0.019	0.038	26
4349.43	O II	2	4350.41	0.020	0.039	25
4361.60	N II		4362.55	0.012	0.023	35
4363.21	[O III]	2F	4364.19	0.968	1.877	5
4366.89	O II	2	4367.90	0.021	0.041	24
4368.19	O I	5	4369.32	0.019	0.037	26
4368.25	O I	5				
4387.93	He I	51	4388.93	0.306	0.574	6
4437.55	He I	50	4438.56	0.043	0.076	16
4471.48	He I	14	4472.52	2.727	4.592	4
4607.13	[Fe III]	3F	4608.13	0.023	0.032	23
4609.44	O II	93	4610.42	0.009	0.012	:
4630.54	N II	5	4631.59	0.026	0.035	22
4638.86	O II	1	4639.90	0.037	0.051	17
4641.81	O II	1	4642.86	0.054	0.073	14
4649.13	O II	1	4650.22	0.071	0.094	12
4650.84	O II	1	4651.87	0.034	0.045	18
4658.10	[Fe III]	3F	4659.18	0.417	0.547	5
4661.63	O II	1	4662.64	0.044	0.057	16
4667.01	[Fe III]	3F	4668.04	0.017	0.022	28
4673.73	O II	1	4674.79	0.009	0.012	:
4676.24	O II	1	4677.34	0.025	0.032	22
4701.53	[Fe III]	3F	4702.65	0.116	0.143	9
4711.37	[Ar IV]	1F	4712.49	0.018	0.023	27
4713.14	He I	12	4714.25	0.501	0.611	5
4733.93	[Fe III]	3F	4734.99	0.042	0.050	16
4740.16	[Ar IV]	1F	4741.32	0.016	0.019	29
4754.83	[Fe III]	3F	4755.82	0.083	0.096	11
4769.60	[Fe III]	3F	4770.55	0.044	0.050	15
4777.88	[Fe III]	3F	4778.81	0.021	0.023	25
4861.33	H I	Hβ	4862.42	100.0	100.0	4
4881	[Fe III]	2F	4882.15	0.180	0.176	7
4889.62	[Fe II]	4F	4890.82	0.014	0.014	31
4894.59	O I		4895.86	0.010	0.010	38
4921.93	He I	48	4923.05	1.202	1.109	4
4924.5	[Fe III]	2F	4925.67	0.024	0.022	22
4931.32	[O III]	1F	4932.36	0.045	0.041	15
4958.91	[O III]	1F	4960.09	139.9	122.8	4
4985.9	[Fe III]	2F	4986.97	0.072	0.061	12
4987.2	[Fe III]	2F	4988.38	0.079	0.067	11
5006.84	[O III]	1F	5008.03	432.8	356.2	4
5011.30	[Fe III]	1F	5012.46	0.063	0.052	12
5015.68	He I	4	5016.86	2.802	2.279	4
5041.03	Si II	5	5042.21	0.100	0.079	10
5055.98	Si II	5	5057.21	0.172	0.133	7
5191.82	[Ar III]	3F	5192.91	0.100	0.064	10
5197.90	[N I]	1F	5199.27	0.149	0.095	8
5200.26	[N I]	1F	5201.69	0.092	0.059	10
5261.62	[Fe II]	19F	5263.00	0.022	0.013	:
5270.40	[Fe III]	1F	5271.75	0.341	0.198	6
5412.00	[Fe III]	1F	5413.40	0.038	0.018	17
5517.71	[Cl III]	1F	5518.98	0.961	0.415	5
5537.88	[Cl III]	1F	5539.13	0.914	0.387	5
5875.64	He I	11	5877.03	32.51	14.44	4
5941.65	N II	28	5943.18	0.036	0.015	17
5978.93	Si II	4	5980.31	0.141	0.057	8
6300.30	[O I]	1F	6301.91	1.164	0.359	4
6312.10	[S III]	3F	6313.55	5.293	1.615	4
6347.11	Si II	4	6348.58	0.505	0.150	5
6363.78	[O I]	1F	6365.40	0.444	0.130	5
6371.36	Si II	2	6372.87	0.260	0.076	6

Table 1. continued

λ_0 (Å)	Ion	Multiplet	λ_{obs} (Å)	$F(\lambda)$	$I(\lambda)$	Error (%)[a]
6548.03	[N II]	1F	6549.61	30.40	7.681	4
6562.82	H I	Hα	6564.31	1161	290.0	4
6578.05	C II	2	6579.60	0.599	0.148	5
6583.41	[N II]	1F	6585.02	96.78	23.79	4
6678.15	He I	46	6679.77	15.34	3.508	4
6716.47	[S II]	2F	6718.03	15.70	3.487	4
6730.85	[S II]	2F	6732.60	18.66	4.101	4
6734.08	He I	1/22	6735.84	0.025	0.005	22
6734.42	[Fe IV]					
6739.8	[Fe IV]		6741.65	0.014	0.004	31
6744.1	He I	1/22	6745.93	0.011	0.003	37
6755.95	He I	1/20	6757.60	0.013	0.004	33
6755.99	[Fe IV]					
6785.68	He I	1/18	6787.67	0.020	0.005	25
6787.21	C II	14	6788.84	0.010	0.003	:
6791.47	C II	14	6793.15	0.011	0.003	37
6804.95	He I	1/17	6806.75	0.025	0.007	22
6855.88	He I	1/15	6857.73	0.023	0.006	23
6933.99	He I	1/13	6935.78	0.031	0.008	19
6989.53	He I	1/12	6991.31	0.051	0.012	14
7062.34	He I	1/11	7064.10	0.085	0.019	11
7065.28	He I	10	7066.90	26.66	5.885	4
7135.78	[Ar III]	1F	7137.45	65.90	13.87	4
7155.16	[Fe II]	14F	7157.11	0.088	0.018	10
7160.56	He I	1/10	7162.42	0.135	0.028	8
7231.32	C II	3	7233.25	0.180	0.036	7
7236.42	C II	3	7238.15	0.508	0.100	5
7281.35	He I	45	7283.06	3.512	0.671	4
7298.04	He I	1/9	7299.84	0.102	0.019	10
7318.39	[O II]	2F	7320.77	4.099	0.765	4
7319.99	[O II]	2F	7321.85	13.18	2.455	4
7329.66	[O II]	2F	7331.41	6.969	1.291	4
7330.73	[O II]	2F	7332.49	7.297	1.351	4
7377.83	[Ni II]	2F	7379.90	0.123	0.022	9
7423.64	N I	3	7425.70	0.022	0.004	24
7442.3	N I	3	7444.39	0.070	0.012	12
7452.54	[Fe II]	14F	7454.55	0.033	0.006	19
7499.85	He I	1/8	7501.77	0.238	0.040	6
7504.94	O II		7506.86	0.020	0.0033	25
7513.33	He I		7515.25	0.017	0.0028	28
7519.29	He I		7521.52	0.036	0.006	17
7519.49	C II	16.8				
7519.93	C II	16.8				
7530.54	[Cl IV]	1F	7532.51	0.027	0.0043	21
7530.57	C II	16.8				
7751.10	[Ar III]	2F	7752.92	20.94	3.001	4
7774.17	O I	1	7776.17	0.031	0.0044	19
7775.39	O I	1	7777.32	0.017	0.0024	28
7816.13	He I	1/7	7817.98	0.402	0.055	4
8015.96	He I	4/20	8017.94	0.024	0.0029	23
8035.06	He I	4/19	8037.14	0.038	0.0047	17
8045.62	[Cl IV]	1F	8047.82	0.59	0.0072	13
8057.55	He I	4/18	8059.50	0.042	0.0051	16
8094.11	He I	4/10	8096.18	0.039	0.0046	17
8116.44	He I	4/16	8118.45	0.049	0.0058	14
8203.86	He I	4/14	8205.98	0.113	0.0126	9
8210.72	N I	2	8213.11	0.045	0.0051	15
8216.34	N I	2	8218.82	0.078	0.0087	11
8223.14	N I	2	8225.21	0.206	0.023	7
8233.21	H I	P50	8235.13	0.090	0.0100	10
8234.43	H I	P49	8236.39	0.114	0.0125	9
8235.74	H I	P48	8237.71	0.113	0.0124	9

Table 1. continued

λ_0 (Å)	Ion	Multiplet	λ_{obs} (Å)	$F(\lambda)$	$I(\lambda)$	Error (%)[a]
8237.13	H I	P47	8239.05	0.183	0.020	7
8238.61	H I	P46	8240.55	0.202	0.022	7
8240.19	H I	P45	8242.02	0.283	0.031	6
8241.88	H I	P44	8244.12	0.304	0.033	6
8243.69	H I	P43	8245.60	0.274	0.030	6
8245.64	H I	P42	8247.56	0.379	0.042	5
8247.73	H I	P41	8249.66	0.346	0.038	5
8249.2	H I	P40	8251.89	0.343	0.038	5
8252.4	H I	P39	8254.35	0.404	0.044	5
8255.02	H I	P38	8257.04	0.319	0.035	6
8257.85	H I	P37	8259.82	0.367	0.040	5
8260.93	H I	P36	8262.84	0.460	0.050	5
8264.28	H I	P35	8266.28	0.660	0.072	5
8265.7	He I	2/9	8267.71	0.055	0.0059	14
8267.94	H I	P34	8269.89	0.555	0.060	5
8271.93	H I	P33	8273.80	0.512	0.055	5
8276.31	H I	P32	8278.33	1.543	0.167	4
8281.12	H I	P31	8283.03	0.865	0.093	5
8290.56	He I	6/27	8292.71	0.025	0.0027	22
8292.31	H I	P29	8294.28	0.597	0.064	5
8298.83	H I	P28	8300.82	0.785	0.084	5
8306.11	H I	P27	8308.06	1.067	0.114	4
8314.26	H I	P26	8316.22	1.055	0.112	4
8323.42	H I	P25	8325.39	1.290	0.136	4
8329.86	He I	6/23	8331.76	0.038	0.0040	17
8333.78	H I	P24	8335.76	1.396	0.146	4
8345.55	H I	P23	8347.51	1.599	0.167	4
8359.00	H I	P22	8360.93	2.018	0.209	4
8361.73	He I	1/6	8363.81	0.822	0.085	5
8374.48	H I	P21	8376.43	1.994	0.205	4
8376.56	He I	6/20	8378.62	0.066	0.0068	12
8392.40	H I	P20	8394.36	2.325	0.237	4
8413.32	H I	P19	8415.24	4.827	0.487	4
8421.97	He I	6/18	8424.04	0.118	0.012	9
8862.79	H I	P11	8862.50	11.71	1.410	4
8914.77	He I	2/7	8917.12	0.119	0.014	9
8930.77	He I	10/11	8933.30	0.044	0.0051	15
8996.99	He I	6/10	8998.67	0.489	0.056	5
9014.91	H I	P10	9017.24	7.810	0.882	4
9063.32	He I	4/8	9065.61	0.466	0.052	5
9068.90	[S III]	1F	9071.05	198.7	21.94	4
9123.6	[Cl II]	1F	9126.03	0.131	0.014	8
9210.28	He I	6/9	9212.52	0.635	0.066	5
9213.24	He I	7/9	9215.60	0.239	0.025	6
9229.01	H I	P9	9231.26	19.40	2.008	4
9262.67	O I	8	9265.07	0.021	0.0021	25
9265.94	O I	8	9268.33	0.031	0.0031	19
9463.57	He I	1/5	9465.78	1.120	0.106	4
9526.17	He I	6/8	9528.41	0.465	0.043	5
9530.60	[S III]	1F	9532.95	520.5	48.02	4
9545.97	H I	P8	9548.06	27.04	2.48	4
9625.70	He I	6/8	9628.23	0.207	0.019	7
9682.39	He I	9/8	9685.01	0.041	0.0036	16
9701.87	[Fe III]		9704.40	0.131	0.0113	8
9702.65	He I	75	9705.29	0.172	0.015	7
9903.46	C II	17.2	9906.40	0.389	0.032	6
10027.70	He I	6/7	10030.66	2.050	0.159	4
10031.2	He I	7/7	10033.94	0.657	0.051	5
10049.40	H I	P7	10051.76	57.70	4.450	4
10138.42	He I	10/7	10140.91	0.247	0.019	6

[a] Error of the dereddened flux ratios. Colons indicate errors larger than 40 per cent.

4 PHYSICAL CONDITIONS AND CHEMICAL ABUNDANCES OF NGC 2579

The physical conditions of the ionised gas: electron temperature, T_e, and density, n_e, have been derived from the usual CEL ratios, using the IRAF task `temden` of the package NEBULAR (Shaw & Dufour 1995) with the atomic dataset compiled by García-Rojas et al. (2005). Electron densities have been derived from [N I] $\lambda\lambda$5198/5200, [O II] $\lambda\lambda$3726/3729, [S II] $\lambda\lambda$6717/6731, [Cl III] $\lambda\lambda$5518/5538, and [Ar IV] $\lambda\lambda$4711/4740 line ratios. We have also determined n_e from the line ratios of several [Fe III] lines following the procedure described by García-Rojas et al. (2006). Electron temperatures have been calculated using several sets of auroral to nebular line intensity ratios: [O II] $\lambda\lambda$7319, 7330/[O II] $\lambda\lambda$3726, 3729, [S II] $\lambda\lambda$4069, 4076/[S II] $\lambda\lambda$6717, 6731, [O III] λ4363/[O III] $\lambda\lambda$4959, 5007, [S III] λ6312/[S III] $\lambda\lambda$9069, 9532 and [Ar III] λ5192/[Ar III] $\lambda\lambda$7136, 7751. Unfortunately, it was not possible to calculate T_e([N II]) because the auroral [N II] λ5755 Å line was in an incomplete spectral order.

The procedure for the determination of the physical conditions was the following: an initial T_e-value of 8,000 K was assumed in order to derive a first approximation to the different n_e determinations; then these preliminary n_e-values were used to recompute T_e, and finally, we iterated until convergence to obtain the final adopted values of n_e and T_e. T_e([O II]) has been corrected from the contribution to [O II] $\lambda\lambda$7319, 7330 due to recombination following the formulae derived by Liu et al. (2000). This correction only contributes a 2.4% to the intensity of [O II] $\lambda\lambda$7319, 7330 lines. The physical conditions determined for NGC 2579 are shown in Table 2.

NGC 2579 present a non-uniform density structure. Copetti et al. (2000, 2007) showed that the n_e([S II]) presents a strong spatial variation, with the density ranging from about 1800 cm^{-3} at the brightest eastern-central areas to less than 100 cm^{-3} at the outer parts of the nebula. This density variation was interpreted as steep radial gradient, similar to that found in the Orion Nebula (Osterbrock & Flather 1959). However, the density estimates listed in Table 2 are rather similar and between 1000 and 2000 cm^{-3}. Copetti et al. (2007) obtained n_e([S II]) $\approx$ 1200 cm^{-3} at the position of the present observations and an upper limit of n_e([Cl III]) of about 2100 cm^{-3} from the integrated spectrum. Those authors derive values of T_e([N II]) and T_e([O III]) of 11000 and 9000 K, respectively, consistent with our determinations.

Ionic abundances of N^+, O^+, O^{2+}, Ne^{2+}, S^+, S^{2+}, Cl^+, Cl^{2+}, Cl^{3+}, Ar^{2+} and Ar^{3+} have been derived from CELs under the two-zone scheme and $t^2 = 0$, using the NEBULAR package, except in the case of Cl^+ for which we have used another analysis package (see below). We have assumed T_e([O II]) for the abundance calculations of low ionization potential ions: N^+, O^+ and S^+; and T_e([O III]) for the high ionization potential ones: O^{2+}, Ne^{2+}, S^{2+}, Cl^{2+}, Ar^{2+} and Ar^{3+}. We have adopted $n_e = 1360 \pm 170$ for all the ions. This value is the weighted mean of the densities obtained from [S II], [O II] and [Cl III] line ratios. For Ne^{2+} we have used the updated atomic data listed in García-Rojas et al. (2009) instead of those included by default in NEBULAR. The older atomic dataset gave an inconsistency of about 0.15 dex in the abundances obtained from the two [Ne III] lines observed.

Table 2. Physical Conditions of NGC 2579.

	Lines	Value
n_e (cm^{-3})	[N I]	1500±700
	[O II]	1570±280
	[S II]	1140±230
	[Fe III]	2330±800
	[Cl III]	1900±600
	[Ar IV]	1670^{+4900}_{-1670}
T_e (K)	[O II]	10450±250
	[S II]	7840±360
	[O III]	9410±160
	[S III]	10760±230
	[Ar III]	8650±280

Many [Fe III] lines have been detected in the spectrum of NGC 2579. We have calculated the Fe^{2+}/H^+ ratio using a 34-level model atom that includes the collision strengths from Zhang (1996), transition probabilities of Quinet (1996) as well as the transitions found by Johansson et al. (2000). The average value of Fe^{2+} abundance has been obtained from 12 individual emission lines and assuming T_e([O II]) as the representative temperature for this ion. We have detected [Fe II] 4287 Å, the only line of this ion present in our spectrum. The intensity of this line is affected by continuum or starlight fluorescence (see Rodríguez 1999) and therefore we can not determine an accurate abundance from this line. Unfortunately, the brightest and less sensitive to fluorescence [Fe II] line, [Fe II] 8616 Å is in one of our observational gaps. Several [Fe IV] lines have been detected in NGC 2579 however only [Fe IV] 6739.8 Å is not blended with other lines. Using that single line, the Fe^{3+}/H^+ ratio has been derived using a 33-level model atom where all collision strengths are those calculated by Zhang & Pradhan (1997) and the transition probabilities recommended by Froese Fischer et al. (2008). We have asummed T_e([O III]) to derive the Fe^{3+} abundances. The Cl^+ abundance cannot be derived from the NEBULAR routines, instead we have used PYNEB (Luridiana et al. 2012), which is an updated version of the NEBULAR package written in PYTHON programming language. For Cl^+ we have used the line wavelengths and energy levels obtained by Radziemski & Kaufman (1974), the transition probabilities compiled by Mendoza (1983) and the collision strengths from Tayal (2004). Ionic abundances are presented in Table 3.

We have measured several He I emission lines in the spectrum of NGC 2579. These lines arise basically from recombination but they can be affected by collisional excitation and self-absorption effects. We have used the effective recombination coefficients of Porter et al. (2005) – with the interpolation formulae provided by Porter et al. (2007) – for He I as well as those of Storey & Hummer (1995) for H I, in order to calculate the He^+ abundance. The collisional contribution was estimated from Sawey & Berrington (1993) and Kingdon & Ferland (1995), and the optical depth in the triplet lines were derived from the computations by Benjamin et al. (2002). We have determined the He^+/H^+ ratio from a maximum likelihood method (MLM, Peimbert et al. 2000, 2002).

To determine the He^+/H^+ ratio, T_e(He I), the temperature fluctuations parameter (Peimbert 1967) for He I,

Table 3. Ionic and total abundances[a]

	This work		C07[b]
	$t^2 = 0.000$	$t^2 = 0.045 \pm 0.007$	$t^2 = 0.000$
Ionic abundances from CELs[c]			
N^+	6.62±0.02	6.75±0.03	6.63±0.12
O^+	7.70±0.03	7.84±0.03	7.65±0.16
O^{2+}	8.19±0.02	8.46±0.03	8.31±0.06
Ne^{2+}	7.23±0.03	7.53±0.06	7.59±0.08
S^+	5.24±0.02	5.36±0.03	5.30±0.12
S^{2+}	6.54±0.02	6.84±0.06	6.78±0.08
Cl^+	3.38±0.04	3.49±0.06	–
Cl^{2+}	4.80±0.02	5.06±0.05	5.03±0.05
Cl^{3+}	2.78±0.07	3.01±0.10	–
Ar^{2+}	6.14±0.02	6.37±0.04	–
Ar^{3+}	3.66±0.09	3.94±0.10	–
Fe^{2+}	5.27±0.10	5.40±0.10	–
Fe^{3+}	5.14±0.29	5.37±0.30	–
Ionic abundances from RLs[d]			
He^+	10.94±0.01		10.96±0.04
C^{2+}	8.13±0.05		–
O^+	7.85±0.07		–
O^{2+}	8.46±0.03		–
Total abundances from CELs[c]			
N	7.31±0.04	7.54±0.05	7.37±0.06
O	8.31±0.02	8.55±0.03	8.39±0.05
Ne	7.35±0.02	7.62±0.07	7.68±0.06
S	6.64±0.02	6.93±0.06	6.91±0.11
Cl	4.82±0.02	5.08±0.05	5.16±0.08
Ar	6.17±0.02	6.38±0.04	–
Fe	5.74±0.08	5.94±0.08	–
Total abundances from RLs[d]			
He	10.96±0.01		10.96±0.04
C	8.30±0.05		–
O	8.56±0.03		–

[a] In units of $12+\log(X^{+n}/H^+)$.

[b] Copetti et al. (2007).

[c] CELs: Collisionally excited lines.

[d] RLs: Recombination lines.

t^2(He I), and the optical depth in the He I λ3889 line, τ_{3889}, in a self-consistent manner, we have used the adopted density obtained from the CEL ratios (see Table 2), and a set of 16 I(He I)/I(H I) line ratios ($\lambda\lambda$ 3614, 3819, 3889, 3965, 4026, 4121, 4388, 4471, 4713, 4922, 5016, 5048, 5876, 6678, 7065, 7281 Å). We have obtained the best sets of values of the three unknowns by minimizing χ^2. The lowest χ^2 parameters we obtain are in the range from 14 to 28, which indicate reasonably good fits. The final adopted He^+ abundance is $12+\log(He^+/H^+) = 10.94 \pm 0.01$ (see Table 3). Interestingly, the range of values of t^2(He I) we obtain in these fits is between 0.025 and 0.065, consistent with that obtained assuming that the ADF(O^{2+}) is produced by the presence of temperature fluctuations in the ionised gas (see below).

We have detected several C II lines in our spectrum, but most of them are produced by resonance fluorescence by starlight (Esteban et al. 1998, 2004). Only C II 4267 and 9903 Å are pure RLs and permit to derive the C^{2+}/H^+ ratio. Two RLs of multiplet 1 of O I are detected in the red part of the spectrum, namely O I 7774 and 7775 Å, and fortunately these important lines are not affected by telluric emission. We also detect and measure a large number of RLs of O II. In particular, seven lines of multiplet 1, four of multiplet 2 and three of multiplet 10 that are produced by pure recombination and can be used to derive the O^{2+}/H^+ ratio. We have used T_e([O III]) and the effective recombination coefficients of Davey et al. (2000) for C II and Storey (1994) for O II to determine the C^{2+} and O^{2+} abundances; and T_e([O II]) and the effective recombination coefficients of Escalante & Victor (1992) and Péequignot et al. (1991) for the O^+ abundance. The C^{2+} abundance obtained from the C II 4267 and 9903 Å lines are $12 + \log (C^{2+}/H^+) = 8.18 \pm 0.05$ and 8.10 ± 0.03, respectively. We adopted the weighted mean of both values for the final C^{2+} abundance included in Table 3. In the case of the O^+/H^+ we adopted the mean value of the abundances obtained from each of the two lines detected and the two sets of effective recombination coefficients indicated above. Following our usual methodology to minimize uncertainties, we have derived the O^{2+} abundance from the estimated total flux of each multiplet (see Esteban et al. 1998). In particular, we obtain values of $12+\log(O^{2+}/H^+) = 8.46\pm0.03$, 8.51±0.06 and 8.40±0.07 for multiplets 1, 2 and 10 respectively, remarkably similar and consistent within the errors. We have assumed the abundance obtained from multiplet 1 as the representative one for O^{2+} (a weighted mean value of the abundances given by each multiplet gives almost the same value). Our spectrum also shows a relatively large number of permitted lines of other heavy-element ions (N II, O I and Si II) but they are not produced by pure recombination and we can not derive reliable abundances from them (see Esteban et al. 1998, 2004).

Our deep spectrum permits to calculate O^+ and O^{2+} abundances from two kinds of lines – RLs and CELs. As for all H II regions where both kinds of lines have been observed (e.g. García-Rojas & Esteban 2007; Esteban et al. 2009), the abundance determined from RLs is larger than that obtained from CELs. Then, we can compute the so-called abundance discrepancy factor for O^+ and O^{2+}, ADF(X^i) , which is defined in its logarithmic form as:

$$\mathrm{ADF}(X^i) = \log(X^i/H^+)_{\mathrm{RLs}} - \log(X^i/H^+)_{\mathrm{CELs}}. \quad (1)$$

The value of the ADF(O^{2+}) we obtain for NGC 2579 is 0.27 ± 0.03, remarkably similar to the values of this quantity found for other Galactic and extragalactic H II regions, which mean value is 0.26 ± 0.09 (Esteban et al. 2009). In the case of O^+, we obtain ADF(O^+) = 0.15 ± 0.08, which is also in excellent agreement with the values of between 0.15 and 0.20 we obtain for other well observed Galactic H II regions as M 8, M 20 and the Orion nebula (García-Rojas & Esteban 2007).

If – as an hypothesis – we assume the validity of the temperature fluctuations paradigm and that this phenomenon produces the abundance discrepancy (see García-Rojas & Esteban 2007), we can estimate the t^2 parameter that produces the agreement between the abundance of O^{2+} determined from CELs and RLs, which results to be $t^2 = 0.045 \pm 0.007$. In Table 3 we include ionic abundances determined for $t^2 = 0$ – the standard procedure considering no temperature fluctuations – and assuming t^2

= 0.045 ± 0.007. These last calculations have been made following the formalism outlined by Peimbert & Costero (1969). It is remarkable that the t^2 parameter value we obtain from the comparison of O^+ abundances determined from CELs and RL is 0.048 ± 0.029, in excellent agreement with the value we obtain for O^{2+}. This consistency supports that the phenomenon that produce the abundance discrepancy and temperature fluctuations may be connected or even be the same, at least in H II regions (see discussion in García-Rojas & Esteban 2007).

We have adopted a set of ionization correction factors (ICFs) to correct for the unseen ionization stages and derive the total gas phase abundances of the different elements, except in the cases of O and Cl, for which we have measured emission lines of all the expected ionic species of these elements. The final total abundances for $t^2 = 0$ and $t^2 = 0.045 \pm 0.007$ are presented in Table 3. For He, C, N, S and Ne we have adopted the same ICF schemes used by García-Rojas & Esteban (2007) in order to facilitate the comparison with data of other Galactic H II regions and study the abundance gradients. The total helium abundance has been corrected for the presence of neutral helium using the expression proposed by Peimbert et al. (1992) based on the similarity of the ionization potentials of He^0 and S^+. In the case of C we have adopted the ICF(C^+) derived from photoionization models of Garnett et al. (1999). In order to derive the total abundance of nitrogen we have used the ICF derived from the models by Mathis & Rosa (1991); note that these ICF values yield N abundances about 0.11 dex higher than those obtained from the usual formulation by Peimbert & Costero (1969) based on the similarity of the ionization potential of N^+ and O^+. The total abundance of oxygen is calculated as the sum of O^+ and O^{2+} abundances. The only measurable CELs of Ne in the optical range are those of Ne^{2+} but the fraction of Ne^+ may not be negligible in the nebula. We have adopted the usual expression of (Peimbert & Costero 1969) to obtain the total Ne abundance. This scheme seems to be apropriate for the ionization degree of NGC 2579. We have measured CELs of two ionization stages of S: S^+ and S^{2+}, and used the ICF proposed by Stasińska (1978) to take into account the presence of some S^{3+}. Chlorine shows lines of the three ionization stages we expect in NGC 2579. Its total abundance is simply the sum of the ionic abundance Cl^+, Cl^{2+} and Cl^{3+}. For argon, we have determinations of Ar^{2+} and Ar^{3+} but some contribution of Ar^+ is also expected. We have adopted the ICF recommended by Izotov et al. (1994) for this element. Finally, we have used an ICF scheme based on photoionization models of Rodríguez & Rubin (2005) to obtain the total Fe/H ratio. In Table 3 we include the total abundances determined for $t^2 = 0$ and $t^2 = 0.045 \pm 0.007$. The variations due to the dependence of the adopted ICFs on the t^2 considered are also included in the total abundances given in Table 3.

In Table 3 we also include the ionic and total abundances obtained by Copetti et al. (2007) for their ABC spectrum of NGC 2579. Those authors do not consider temperature fluctuations. We can see that all abundances of twice ionised species determined by Copetti et al. (2007) are somewhat larger than our determinations. This fact is perhaps indicating that both sets of observations correspond to nebular areas with somewhat different integrated ionization conditions. However, the total abundances obtained in both studies are in general consistent except in the case of Ne and Cl, where the difference is 0.33 and 0.34 dex, respectively. The discrepancy in Ne/H ratios is due to the large difference between the intensities of the [Ne III] lines reported in both datasets. In the case of Cl/H the difference could be due to the different methodology used by Copetti et al. (2007) and us for determining the abundance of this element. Those authors use Cl^{2+}/H^+ and an ICF and we determine Cl/H directly from the sum of the different ionic abundances.

It is interesting to compare the abundance ratios determined for NGC 2579 with those of reference objects. In Table 4 we show the C/O, N/O, Ne/O, S/O, Cl/O and Ar/O measured for NGC 2579 in the case of assuming $t^2 = 0$ and $t^2 = 0.045$, the abundance ratios for the solar photosphere (Asplund et al. 2009) – the protosolar values are identical – and the values obtained for the Orion nebula (García-Rojas & Esteban 2007, assuming $t^2 > 0$). In general, we can see that the ratios are rather consistent in the 3 objects within the errors. The value we obtain of log(Ne/O) ~ -0.93 is somewhat low, even lower than the typical ratio of about -0.70 found for extragalactic H II regions covering a very wide range of metalicity (Dors et al. 2013). This indicates that our determination of Ne^{++}/H^+ and Ne/H is probably about 0.20 lower than expected. In the case of the N/O ratio, it is consistent with that obtained by Copetti et al. (2007) within the errors, but about 0.17 dex lower than that of the Orion nebula.

5 CHEMICAL EVOLUTION MODEL AND DISCUSSION

The derivation of precise abundances for NGC 2579 is an opportunity to explore the behaviour of the radial abundance gradients of ionised gas at galactocentric distances larger than the solar ones. In Figure 3 we include the C/H, O/H and C/O ratios of NGC 2579 as those for the sample of H II regions of García-Rojas & Esteban (2007), which are also determined using the intensity of RLs and the same methodology. The objects of that sample are located at galactocentric distances between 6.3 and 10.4 kpc (assuming the Sun at 8 kpc). We also include the radial gradients determined from the linear fit to the data sample of García-Rojas & Esteban (2007) but extrapolated up to 13 kpc. As it can be seen in Figure 3, the point of NGC 2579 stands above the extrapolated gradients, specially in the case of the C and C/O gradients. Assuming that the distance to this object is well established (that seems to be the case, see discussion of section 5.2 of Copetti et al. 2007), our data indicate that the chemical behaviour of NGC 2579 does not fit the trend of the inner Galactic H II regions. Although we deal with data of a single object – and obviously lacking statistical significance – this result indicates that the chemical composition of NGC 2579 is consistent with flatten gradients at its galactocentric distance. Another interesting feature of Figure 3 is that the C/O gradient seems to be better represented by a step function instead of a linear fit. Regions with $R_G < 7.3$ kpc show log(C/O) ratios of the ionised gas of about 0.0 but regions farther out from the Galactic Centre can be represented by a constant value around -0.26 with a rather small statistical dispersion.

Table 4. Comparison of abundance ratios

	NGC 2579			Orion neb.[b]
	$t^2 = 0$	$t^2 > 0$	Sun[a]	$t^2 > 0$
C/O	–	−0.26±0.06	−0.26±0.07	−0.28±0.04
N/O	−1.00±0.04	−1.01±0.06	−0.86±0.07	−0.84±0.10
Ne/O	−0.96±0.02	−0.93±0.08	−0.76±0.11	−0.77±0.08
S/O	−1.67±0.02	−1.62±0.07	−1.57±0.06	−1.48±0.05
Cl/O	−3.47±0.02	−3.47±0.06	−3.19±0.33	−3.42±0.05
Ar/O	−2.14±0.02	−2.17±0.05	−2.29±0.14	−2.08±0.07

[a] Asplund et al. (2009) .

[b] García-Rojas & Esteban (2007).

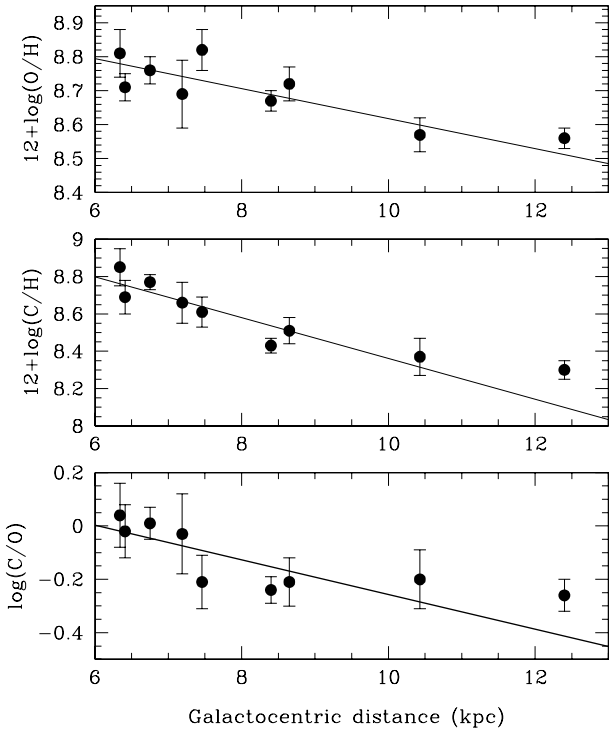

Figure 3. Ionised gas phase O, C and C/O radial abundance gradients of the Galactic disc from H II region abundances determined from recombination lines. The point at 12.4 kpc corresponds to NGC 2579, the rest are taken from García-Rojas & Esteban (2007). The lines indicate the radial gradients obtained from the linear fit of the data between 6.3 to 10.4 kpc and extrapolated to 13 kpc. The Sun is located at 8 kpc.

Some authors have claimed – based on both H II regions and planetary nebulae data – that gas phase radial abundance gradients may flatten out at the outer parts of the Galactic disc (Fich & Silkey 1991; Vílchez & Esteban 1996; Maciel & Quireza 1999; Costa et al. 2004; Maciel et al. 2006), although other authors do not support such flattening (Deharveng et al. 2000; Rudolph et al. 2006; Henry et al. 2010; Balser et al. 2011). Metallicity determinations of other kinds of objects, such as Cepheids (Luck et al. 2003; Andrievsky et al. 2004; Yong et al. 2006; Pedicelli et al. 2009) and Galactic open clusters (Twarog et al. 1997; Yong et al. 2012), provide further evidence of such change of slope of the gradients at large distances. Strong evidence for flat radial gradients from the spectra of H II regions in the outer discs of nearby spiral galaxies has been presented in several recent papers by Bresolin et al. (2009) for M83, Goddard et al. (2011) for NGC 4625, Bresolin et al. (2012) for NGC 1512 and NGC 3621 and Werk et al. (2011) for a sample of 13 – mostly interacting – galaxies. Moreover, a flattening or an upturn of the metallicity gradient has also been found from stellar photometry of red giant branch stars in the outer disc of the spiral galaxies NGC 300 and NGC 7793 (Vlajić et al. 2009, 2011). The value of 12+log(O/H) – obtained from the intensity of CELs – in the outer discs of the above mentioned galaxies ranges between 8.2 and 8.4 (Bresolin et al. 2012), consistent with the value of 8.31 ± 002 we derive for NGC 2579. Bresolin et al. (2012) indicate that the flattening of the radial abundance in external spiral galaxies occurs approximately at the isophotal radius, R_{25}. In the case of the Milky Way, R_{25} is difficult to estimate. The available determinations give values of 11.5 kpc (de Vaucouleurs & Pence 1978) or 13.4 kpc (Goodwin et al. 1998), close to the galactocentric distance determined by Copetti et al. (2007) for NGC 2579. Metallicity studies based on Cepheids and open clusters indicate that the change of the slope of the Fe/H ratio occurs at about 9 kpc (Lépine et al. 2011).

We have made a first exploration of the possible reasons of the flattening of the abundance gradients in the outer galactic discs building a tailored chemical evolution model. Bresolin et al. (2012) discuss several mechanisms that can produce such phenomenon: flattening of the star formation efficiency, radial metal mixing or enriched infall. In this paper, we focus our attention on the first possibility because it is the simplest one to implement in our available models. The model we have used is almost identical to the intermediate wind yields one (IWY), explained in details by Carigi & Peimbert (2011). That IWY model was built to match three observational constraints along the Galactc disc: the radial distributions of the surface density of the total baryonic mass, $M_{\rm tot}(r)$, and gas mass, $M_{\rm gas}(r)$, and the radial gradient of the O/H ratio defined by H II regions of the Milky Way located between 6.3 and 10.4 kpc and derived using RLs.

The main assumptions and ingredients of the IWY model are described in the following. The Milky Way disc was formed in an inside-out scenario from primordial infall with time scales $\tau = r$(kpc) −2 Gyr. The initial mass function is that by Kroupa et al. (1993) in the

0.08 − 80 $M_\odot$ range. We consider an array of metal dependent yields: (a) for low and intermediate mass stars ($0.8 \leqslant m/M_\odot \leqslant 8$), we use the yields by Marigo et al. (1996, 1998) and Portinari et al. (1998); (b) for binary stars ($3 \leqslant m_{bin}/M_\odot \leqslant 16$), we adopted the yields by Nomoto et al. (1997) in SNIa formulation by Greggio & Renzini (1983). We used $A_{bin} = 0.08$, as the fraction of binary stars that are progenitors of SNIa; (c) for massive stars ($8 \leqslant m/M_\odot \leqslant 80$) we considered the yields including stellar rotation by Hirschi (2007) and Meynet & Maeder (2002) for $Z \leqslant 0.004$; and the intermediate wind yields, obtained as an average of the yields by Maeder (1992, high mass-loss rate) and Hirschi et al. (2005, low mass-loss rate)) for $Z = 0.02$. Since Fe yields are not computed by the Geneva group, we adopted Woosley & Weaver (1995) values, following Carigi & Hernandez (2008) prescription.

Our model differs from IWY only in the assumption of a variable star formation process efficiency, ν, for the outer galactocentric radius. With this parameter, the star formation rate, SFR, is a spatial and temporal function of the form

$$\mathrm{SFR}(r,t) = \nu(r) \times M_{\mathrm{gas}}^{1.4}(r,t) \times (M_{\mathrm{gas}} + M_{\mathrm{star}})^{0.4}(r,t); \quad (2)$$

where M_{star} is the surface mass density of stars. The formation process efficiency ν was kept constant in the IWY model, while in the present paper we assume that ν depends on the galactocentric radius. This is the only difference between the IWY model and the present one. We adopt $\nu = 0.016 \equiv \nu_{\mathrm{in}}$ for $r < 10$ kpc and $\nu/\nu_{\mathrm{in}} = 0.8$, 1.3 and 2.2 for r =10, 12 and 14 kpc, respectively. The values of ν as a function of the galactocentric radius we have chosen are those that reproduce the behaviour of O/H radial gradient at large galactocentric radii.

In Figure 4, the model is compared to observational constraints, as follows:

a) $M_{gas}(r)$ values are obtained by adding the atomic and molecular data from figure 7 by Kennicutt & Evans (2012). These original data include the hydrogen and helium components.

b) $SFR(r)$ values are taken from the same figure 7 by Kennicutt & Evans (2012).

c) The disc scale length, R_d, of the Galactic stellar disc ($M_{star}(r) \propto e^{-r/R_d}$) by Yin et al. (2009). In their table 7 they show R_d values between 2.3 and 5 kpc for K, R, V and B bands.

d) O/H and C/H values from H II regions and computed from RLs (García-Rojas & Esteban 2007, this work). The total gaseous abundances shown in our Table 3 have been modified under the assumption that 35% of the O atoms and 25% of the C atoms are trapped in dust grains (Peimbert & Peimbert 2010), increasing the O/H and C/H values by 0.12 and 0.10 dex, respectively.

e) N/H values computed from CELs and assuming $t^2 > 0$ (García-Rojas & Esteban 2007, this work). We have assumed no dust depletion for N.

f) Fe/H gradients from open clusters and Cepheids by Pedicelli et al. (2009), Luck et al. (2011) and Yong et al. (2012).

It is remarkable the agreement with the observational constraints for $r \geqslant 10$ kpc, specifically with the current C/H, N/H, C/O and N/O abundance gradients (slopes and absolute values) and with the SFR, M_{gas} and M_{star} radial distributions, for which the model was not built at all.

The results of the chemical evolution model we have built in this work indicate that an increase of ν for $r \geqslant 10$ kpc can explain the chemical flattening in the outer Galactic disc. It is important to remark that ν does not represent the star formation efficiency, SFE, defined as $SFE(r) = SFR(r)/M_{gas}(r)$, the SFR per unit of surface mass density of gas. In order to clarify this point, we show in Figure 5 the radial distribution of ν and SFE. In this figure, we note that a constant value of ν at inner radii implies a decrease of SFE and an increase of ν at outer radii implies a flat SFE. A similar behaviour of the $SFE(r)$ was found by Bigiel et al. (2010), based on the combination of atomic hydrogen and far-ultraviolet emission in 17 spiral and 5 dwarf galaxies. They conclude that the SFE in the outer disc ($r > R_{25}$) is flatter compared to the SFE in the inner disc ($r < R_{25}$), due to the increase of the SFR with H I column density. The SFE is the inverse of the gas depletion time, the time requiered for present-day star formation to consume the available gas. The values of SFE we obtain at the outer disc indicate a depletion time of about 7.5 Gyr and that this value becomes almost constant in that part of the Galaxy. Bigiel et al. (2010) find depletion times between 10 to 100 Gyr for their sample of spiral and dwarf galaxies.

As Bresolin et al. (2012) point out, a flat SFE can approximately translate into a flattening of the abundance gradient, using their equation 1:

$$\frac{\mathrm{O}}{\mathrm{H}} = \frac{(y_0 \times t \times \Sigma_{\mathrm{SFR}})}{\mu \times \Sigma_{\mathrm{HI}}} \propto SFE; \quad (3)$$

where y_0 is the net oxygen by mass (0.006, integrated yield obtained from the IWY model, Carigi & Peimbert 2011), $\mu = 11.81$ corresponds to the conversion factor from abundance by number to abundance by mass; t is the timescale for the star formation and Σ_{SFR} and Σ_{HI} are the SFR and H I surface density, respectively. Assuming a constant SFR and gas density and that they have been equal to the present-day values in the last Gyrs, we can estimate t from the equation given above. From Figure 4, at the distance of NGC 2579, we obtain $\Sigma_{SFR} \sim 1\ M_\odot\ \mathrm{pc}^{-2}\ \mathrm{Gyr}^{-1}$ and $\Sigma_{HI} \sim \Sigma_{gas} \sim 8\ M_\odot\ \mathrm{pc}^{-2}$. With these numbers we obtain that the time required to enrich the ISM up to the oxygen abundance of NGC 2579 determined from CELs and adding 0.12 dex due to dust depletion, 12 + log $(\mathrm{O/H})_{\mathrm{CELs}} = 8.43$, is ~ 4.2 Gyr (3.2 Gyr without dust correction). In the case we use the abundance determination based on RLs including dust correction, 12 + log $(\mathrm{O/H})_{\mathrm{RLs}} = 8.67$, the time is ~ 7.5 Gyr (5.7 Gyr without dust correction). Simulations of galaxy formation in a Λ cold dark matter (ΛCDM) universe predict that the outer discs of galaxies could have mean formation times around 4-6 Gyr, while the inner parts should have much longer values, > 10 Gyr (Scannapieco et al. 2008, 2009). Our estimations for the outer Galactic disc are roughly consistent with these predictions. Bresolin et al. (2012) determine enrichment timescales for the external discs of two spiral galaxies, for the apparently isolated spiral NGC 3621 they obtain a time of ~ 10 Gyr, and a comparatively much shorter value – around 2-3 Gyr – for the interacting spiral galaxy NGC 1512.

In an upcoming paper, we explore other factors that may produce flat gradients in the outer Galactic disc, as ho-

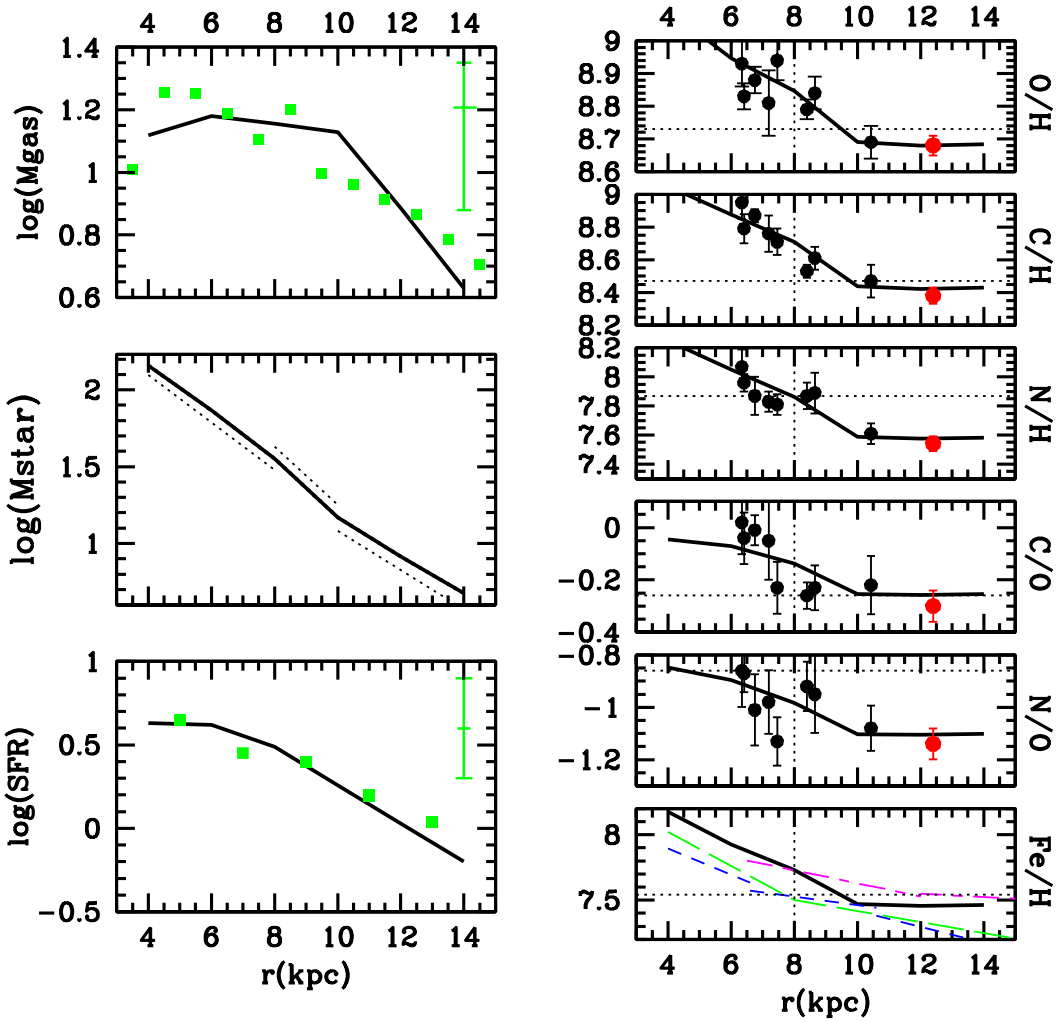

Figure 4. The present-day radial distribution of surface mass densities of gas (M_{gas}) and stars (M_{star}) in $M_{\odot}$ pc^{-2} units and star formation rate (SFR) in $M_{\odot}$ pc^{-2} Gyr^{-1} units (left panels); ISM abundance ratios and stellar Fe/H gradient (right panels). Continuous black lines: Results of the chemical evolution model that assumes an increase of ν for $r \geqslant 10$ kpc. The three dotted lines parallel to the predicted M_{star} correspond to scale lengths (R_d) of 2.8, 2.3 y 3.4 kpc for 4-8 kpc, 8-10 kpc and 10-14 kpc, respectively. Observational data: filled circles represent H II regions (corrected for dust depletion, García-Rojas & Esteban 2007, this work); red circles: NGC 2579 (corrected for dust depletion, this paper); discontinuous lines: Fe/H gradient by Yong et al. (2012, short-long-dashed magenta line), Luck et al. (2011, short-dashed blue line) and Pedicelli et al. (2009, long-dashed green line). Filled green squares: values of M_{gas} and SFR compiled by Kennicutt & Evans (2012). Vertical bars: average observational errors. Diagrams showing O/H, C/H, N/H and Fe/H express the abundances in units of 12+log(X_i/H) and those showing C/O and N/O are in log(X_i/O) units.

mogeneous infall, enriched accretion, and gaseous and stellar radial migration (see Bresolin et al. 2012, for references).

6 CONCLUSIONS

We present deep echelle spectrophotometry in the 3550–10400 Å range of the Galactic H II region NGC 2579. This object is located at a rather large galactocentric distance, 12.4 ± 0.7 kpc (Copetti et al. 2007) and has been largely neglected due to identification problems finally resolved by Copetti et al. (2007). It also shows a rather high surface brightness and ionization degree. All these properties make NGC 2579 an excellent object to explore the behaviour of the Galactic radial abundance gradients of the ionised gas in the outer disc of the Milky Way.

We have derived consistent and precise values of the physical conditions of the nebula making use of several emission line-intensity ratios as well as abundances for several ionic species from the intensity of collisionally excited lines (CELs). Our deep spectra permits – for the first time for a Galactic H II region with so low metallicity – to obtain a very good determination of the ionic C^{2+}, O^{+} and O^{2+} abundances – as well as the total O abundance – from the intensity of faint pure recombination lines (RLs). The comparison between the O^{+}/H^{+} and O^{2+}/H^{+} ratios determined from RLs and CELs gives an abundance discrepancy factor (ADF) of 0.15 ± 0.08 and 0.27 ± 0.03 for O^{+} and O^{2+}, re-

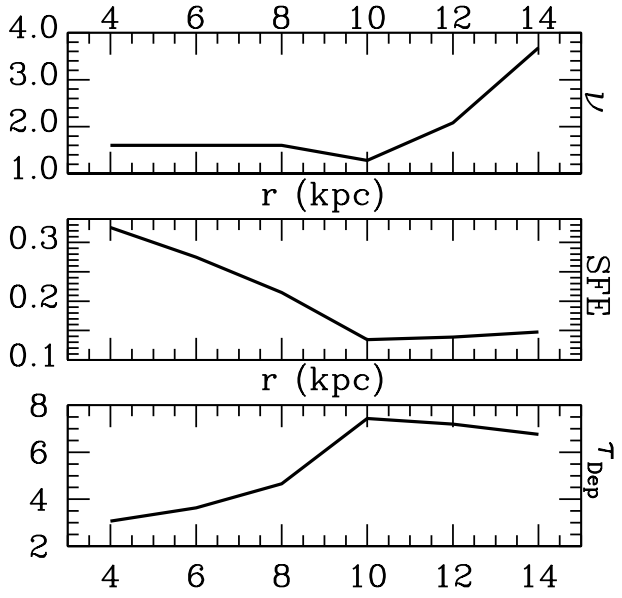

Figure 5. The present-day radial distribution of: ν, where $\nu(r) = SFR(r) \times M_{gas}^{-1.4}(r) \times (M_{gas} + M_{star})^{-0.4}(r)$, in 0.01 $\mathrm{Gyr}^{-1}(M_{\odot}\ \mathrm{pc}^{-2})^{-0.8}$ units (upper panel), the star formation efficiency, $SFE(r) = SFR(r)/M_{gas}(r)$, in Gyr^{-1} units (middle panel) and depletion time $\tau_{\mathrm{Dep}}(r) = 1/SFE(r)$ in Gyr (lower panel).

spectively. Values in complete agreement to the ADFs found for other Galactic and extragalactic H II regions. The value of t^2 that produces the agreement between the O^{2+} abundance determined from CELs and RLs is $t^2 = 0.045 \pm 0.007$, which is consistent to the values we obtain from the comparison of the O^+ abundances – $t^2 = 0.048 \pm 0.029$ – and applying a maximum likelihood method for minimising the dispersion of the He^+/H^+ ratio from individual lines.

Our abundance results for NGC 2579 based on RLs permit to extend the previous determinations of the C, O and C/O gas phase radial gradients of the inner Galactic disc obtained by Esteban et al. (2005) to larger galactocentric distances. We find that the chemical composition of NGC 2579 is consistent with flatten gradients at its galactocentric distance. This result is in agreement with previous claims of flatten outer abundance gradients based on results for ionised nebulae, Cepheids, and open clusters in the Milky Way and with recent results for the outer discs of nearby spiral galaxies.

We have built a chemical evolution model that reproduces the observed radial distributions of O, C and N abundances, the C/O, N/O ratios and other observational constraints, finding that the flattening of abundance gradients in the Milky Way outside the isophotal radius can be explained due to a shallowed star formation efficiency for $r \geqslant 10$ kpc.

ACKNOWLEDGMENTS

We are grateful to the referee, Richard Henry, for comments and suggestions that have improved the paper. This work has been funded by the Spanish Ministerio de Educación y Ciencia (MEC) and Ministerio de Economía y Competitividad (MINECO) under projects AYA2007-63030, AYA2010-16717 and AYA2011-22614. LC thanks the funding provided by CONACyT (grant 129753). MVFC thanks the support of the Brazilian agency CAPES. HOC thanks the support of the IPN provided by the project SIP20121451.

REFERENCES

Acker A., Marcout J., Ochsenbein F., Stenholm B., Tylenda R., 1992, Strasbourg - ESO catalogue of galactic planetary nebulae. Part 1; Part 2

Andrievsky S. M., Luck R. E., Martin P., Lépine J. R. D., 2004, A&A, 413, 159

Archinal B. A., Hynes S. J., 2003, Star clusters

Asplund M., Grevesse N., Sauval A. J., Scott P., 2009, ARA&A, 47, 481

Balser D. S., Rood R. T., Bania T. M., Anderson L. D., 2011, ApJ, 738, 27

Benjamin R. A., Skillman E. D., Smits D. P., 2002, ApJ, 569, 288

Bigiel F., Leroy A., Walter F., Blitz L., Brinks E., de Blok W. J. G., Madore B., 2010, AJ, 140, 1194

Bresolin F., Kennicutt R. C., Ryan-Weber E., 2012, ApJ, 750, 122

Bresolin F., Ryan-Weber E., Kennicutt R. C., Goddard Q., 2009, ApJ, 695, 580

Cardelli J. A., Clayton G. C., Mathis J. S., 1989, ApJ, 345, 245

Carigi L., Hernandez X., 2008, MNRAS, 390, 582

Carigi L., Peimbert M., 2011, Rev. Mexicana Astron. Astrofis., 47, 139

Carigi L., Peimbert M., Esteban C., García-Rojas J., 2005, ApJ, 623, 213

Copetti M. V. F., Mallmann J. A. H., Schmidt A. A., Castañeda H. O., 2000, A&A, 357, 621

Copetti M. V. F., Oliveira V. A., Riffel R., Castañeda H. O., Sanmartim D., 2007, A&A, 472, 847

Costa R. D. D., Uchida M. M. M., Maciel W. J., 2004, A&A, 423, 199

Davey A. R., Storey P. J., Kisielius R., 2000, A&AS, 142, 85

de Vaucouleurs G., Pence W. D., 1978, AJ, 83, 1163

Deharveng L., Peña M., Caplan J., Costero R., 2000, MNRAS, 311, 329

D'Odorico S., Cristiani S., Dekker H., Hill V., Kaufer A., Kim T., Primas F., 2000, in Bergeron J., ed., Society of Photo-Optical Instrumentation Engineers (SPIE) Conference Series Vol. 4005 of Society of Photo-Optical Instrumentation Engineers (SPIE) Conference Series, Performance of UVES, the echelle spectrograph for the ESO VLT and highlights of the first observations of stars and quasars. pp 121–130

Dors Jr. O. L., Hagele G. F., Cardaci M. V., Perez-Montero E., Krabbe A. C., Vilchez J. M., Sales D. A., Riffel R., Riffel R. A., 2013, ArXiv e-prints

Escalante V., Victor G. A., 1992, Planet. Space Sci., 40, 1705

Esteban C., Bresolin F., Peimbert M., García-Rojas J., Peimbert A., Mesa-Delgado A., 2009, ApJ, 700, 654

Esteban C., García-Rojas J., Peimbert M., Peimbert A., Ruiz M. T., Rodríguez M., Carigi L., 2005, ApJ, 618, L95
Esteban C., Peimbert M., García-Rojas J., Ruiz M. T., Peimbert A., Rodríguez M., 2004, MNRAS, 355, 229
Esteban C., Peimbert M., Torres-Peimbert S., Escalante V., 1998, MNRAS, 295, 401
Fich M., Silkey M., 1991, ApJ, 366, 107
Froese Fischer C., Rubin R. H., Rodríguez M., 2008, MNRAS, 391, 1828
Fu J., Hou J. L., Yin J., Chang R. X., 2009, ApJ, 696, 668
García-Rojas J., Esteban C., 2007, ApJ, 670, 457
García-Rojas J., Esteban C., Peimbert A., Peimbert M., Rodríguez M., Ruiz M. T., 2005, MNRAS, 362, 301
García-Rojas J., Esteban C., Peimbert M., Costado M. T., Rodríguez M., Peimbert A., Ruiz M. T., 2006, MNRAS, 368, 253
García-Rojas J., Peña M., Peimbert A., 2009, A&A, 496, 139
Garnett D. R., Shields G. A., Peimbert M., Torres-Peimbert S., Skillman E. D., Dufour R. J., Terlevich E., Terlevich R. J., 1999, ApJ, 513, 168
Goddard Q. E., Bresolin F., Kennicutt R. C., Ryan-Weber E. V., Rosales-Ortega F. F., 2011, MNRAS, 412, 1246
Goodwin S. P., Gribbin J., Hendry M. A., 1998, The Observatory, 118, 201
Greggio L., Renzini A., 1983, A&A, 118, 217
Hamuy M., Suntzeff N. B., Heathcote S. R., Walker A. R., Gigoux P., Phillips M. M., 1994, PASP, 106, 566
Hamuy M., Walker A. R., Suntzeff N. B., Gigoux P., Heathcote S. R., Phillips M. M., 1992, PASP, 104, 533
Henry R. B. C., Kwitter K. B., Jaskot A. E., Balick B., Morrison M. A., Milingo J. B., 2010, ApJ, 724, 748
Hirschi R., 2007, A&A, 461, 571
Hirschi R., Meynet G., Maeder A., 2005, A&A, 433, 1013
Izotov Y. I., Thuan T. X., Lipovetsky V. A., 1994, ApJ, 435, 647
Johansson S., Zethson T., Hartman H., Ekberg J. O., Ishibashi K., Davidson K., Gull T., 2000, A&A, 361, 977
Kaler J. B., 1976, ApJS, 31, 517
Kennicutt R. C., Evans N. J., 2012, ARA&A, 50, 531
Kingdon J., Ferland G. J., 1995, ApJ, 442, 714
Kroupa P., Tout C. A., Gilmore G., 1993, MNRAS, 262, 545
Lépine J. R. D., Cruz P., Scarano Jr. S., Barros D. A., Dias W. S., Pompéia L., Andrievsky S. M., Carraro G., Famaey B., 2011, MNRAS, 417, 698
Liu X.-W., Storey P. J., Barlow M. J., Danziger I. J., Cohen M., Bryce M., 2000, MNRAS, 312, 585
López-Sánchez Á. R., Esteban C., García-Rojas J., Peimbert M., Rodríguez M., 2007, ApJ, 656, 168
Luck R. E., Andrievsky S. M., Kovtyukh V. V., Gieren W., Graczyk D., 2011, AJ, 142, 51
Luck R. E., Gieren W. P., Andrievsky S. M., Kovtyukh V. V., Fouqué P., Pont F., Kienzle F., 2003, A&A, 401, 939
Luridiana V., Morisset C., Shaw R. A., 2012, in IAU Symposium Vol. 283 of IAU Symposium, PyNeb: a new software for the analysis of emission lines. pp 422–423
Maciel W. J., Lago L. G., Costa R. D. D., 2006, A&A, 453, 587
Maciel W. J., Quireza C., 1999, A&A, 345, 629
Maeder A., 1992, A&A, 264, 105
Marcon-Uchida M. M., Matteucci F., Costa R. D. D., 2010, A&A, 520, A35
Marigo P., Bressan A., Chiosi C., 1996, A&A, 313, 545
Marigo P., Bressan A., Chiosi C., 1998, 331, 564
Mathis J. S., Rosa M. R., 1991, A&A, 245, 625
Mendoza C., 1983, in Flower D. R., ed., Planetary Nebulae Vol. 103 of IAU Symposium, Recent advances in atomic calculations and experiments of interest in the study of planetary nebulae. pp 143–172
Mesa-Delgado A., Núñez-Díaz M., Esteban C., García-Rojas J., Flores-Fajardo N., López-Martín L., Tsamis Y. G., Henney W. J., 2012, MNRAS, 426, 614
Meynet G., Maeder A., 2002, A&A, 390, 561
Nicholls D. C., Dopita M. A., Sutherland R. S., 2012, ApJ, 752, 148
Nomoto K., Iwamoto K., Nakasato N., Thielemann F.-K., Brachwitz F., Tsujimoto T., Kubo Y., Kishimoto N., 1997, Nuclear Physics A, 621, 467
Osterbrock D., Flather E., 1959, ApJ, 129, 26
Pedicelli S., et al. 2009, A&A, 504, 81
Péequignot D., Petitjean P., Boisson C., 1991, A&A, 251, 680
Peimbert A., 2003, ApJ, 584, 735
Peimbert A., Peimbert M., 2010, ApJ, 724, 791
Peimbert A., Peimbert M., Luridiana V., 2002, ApJ, 565, 668
Peimbert M., 1967, ApJ, 150, 825
Peimbert M., Costero R., 1969, Boletin de los Observatorios Tonantzintla y Tacubaya, 5, 3
Peimbert M., Peimbert A., Ruiz M. T., 2000, ApJ, 541, 688
Peimbert M., Torres-Peimbert S., Ruiz M. T., 1992, Rev. Mexicana Astron. Astrofis., 24, 155
Péquignot D., Morisset C., Casassus S., 2012, in IAU Symposium Vol. 283 of IAU Symposium, NGC 6302: high-ionization permitted lines. Applying X-SSN synthesis to VLT-UVES spectra. pp 470–471
Porter R. L., Bauman R. P., Ferland G. J., MacAdam K. B., 2005, ApJ, 622, L73
Porter R. L., Ferland G. J., MacAdam K. B., 2007, ApJ, 657, 327
Portinari L., Chiosi C., Bressan A., 1998, A&A, 334, 505
Quinet P., 1996, A&AS, 116, 573
Radziemski Jr. L. J., Kaufman V., 1974, Journal of the Optical Society of America (1917-1983), 64, 366
Rodríguez M., 1999, A&A, 348, 222
Rodríguez M., Rubin R. H., 2005, ApJ, 626, 900
Rudolph A. L., Fich M., Bell G. R., Norsen T., Simpson J. P., Haas M. R., Erickson E. F., 2006, ApJS, 162, 346
Samland M., Hensler G., Theis C., 1997, ApJ, 476, 544
Sawey P. M. J., Berrington K. A., 1993, Atomic Data and Nuclear Data Tables, 55, 81
Scannapieco C., Tissera P. B., White S. D. M., Springel V., 2008, MNRAS, 389, 1137
Scannapieco C., White S. D. M., Springel V., Tissera P. B., 2009, MNRAS, 396, 696
Shaw R. A., Dufour R. J., 1995, PASP, 107, 896
Stasińska G., 1978, A&A, 66, 257
Stasińska G., Tenorio-Tagle G., Rodríguez M., Henney W. J., 2007, aa, 471, 193
Storey P. J., 1994, A&A, 282, 999
Storey P. J., Hummer D. G., 1995, MNRAS, 272, 41
Tayal S. S., 2004, 426, 717

Torres-Peimbert S., Peimbert M., Daltabuit E., 1980, ApJ, 238, 133
Tsamis Y. G., Péquignot D., 2005, MNRAS, 364, 687
Tsamis Y. G., Walsh J. R., Vílchez J. M., Péquignot D., 2011, MNRAS, 412, 1367
Twarog B. A., Ashman K. M., Anthony-Twarog B. J., 1997, AJ, 114, 2556
van den Bergh S., Herbst W., 1975, AJ, 80, 208
Vílchez J. M., Esteban C., 1996, MNRAS, 280, 720
Vlajić M., Bland-Hawthorn J., Freeman K. C., 2009, ApJ, 697, 361
Vlajić M., Bland-Hawthorn J., Freeman K. C., 2011, ApJ, 732, 7
Werk J. K., Putman M. E., Meurer G. R., Santiago-Figueroa N., 2011, ApJ, 735, 71
Woosley S. E., Weaver T. A., 1995, ApJS, 101, 181
Yin J., Hou J. L., Prantzos N., Boissier S., Chang R. X., Shen S. Y., Zhang B., 2009, A&A, 505, 497
Yong D., Carney B. W., Friel E. D., 2012, AJ, 144, 95
Yong D., Carney B. W., Teixera de Almeida M. L., Pohl B. L., 2006, AJ, 131, 2256
Zhang H., 1996, A&AS, 119, 523
Zhang H. L., Pradhan A. K., 1997, A&AS, 126, 373